Mechanical Origin of the Structural Phase Transition in Methylammonium Lead Iodide CH 3 NH 3 PbI 3

ARTICLE *in* JOURNAL OF PHYSICAL CHEMISTRY LETTERS · FEBRUARY 2015

Impact Factor: 7.46 · DOI: 10.1021/jz502740d

4 AUTHORS, INCLUDING:

Khuong P. Ong
Institute Of High Performance Computing
36 PUBLICATIONS **375** CITATIONS

SEE PROFILE

THE JOURNAL OF PHYSICAL CHEMISTRY Letters

Letter

pubs.acs.org/JPCL

Mechanical Origin of the Structural Phase Transition in Methylammonium Lead Iodide $CH_3NH_3PbI_3$

Khuong P. Ong,*[,†] Teck Wee Goh,[‡] Qiang Xu,[†,§] and Alfred Huan[†]

[†]Institute of High Performance Computing, Agency of Science, Technology and Research (A*STAR), 1 Fusionopolis Way, 138632 Singapore

[‡]Division of Physics and Applied Physics, School of Physical and Mathematical Sciences, Nanyang Technological University, 21 Nanyang Link, 637371 Singapore

[§]Entropic Interface Group (EIG), Engineering Product Development, Singapore University of Technology and Design (SUTD), 20 Dover drive, 138682 Singapore

ABSTRACT: The methylammonium lead iodide perovskite ($MAPbI_3$) is presently a desirable material for photovoltaic application. Its structure is orthorhombic at low temperature and tetragonal at room temperature. Most theoretical works have focused on either tetragonal or orthorhombic phase alone leaving a gap in the understanding of the structural phase transition in between. In this work, by ab initio calculations, we elucidate the origin of structural phase transition between these two phases. We show that there exists a critical ratio of out-of-plane to in-plane lattice constants, $c/a \sim 1.45$, where at low c/a the orthorhombic *Pnma* phase is stable while the tetragonal *I4/mcm* phase is stable at high c/a. Varying the c/a ratio leads to a change of PbI_6 octahedral tilting with the rotation of $CH_3NH_3^+$ cations about the NH_3 component in and out of the Oxy plane. The origin of this rotation is identified. We propose that under epitaxial conditions a gradual change in structural phase of the $MAPbI_3$ perovskite may exist and understanding its electronic properties will be beneficial toward the solar cell community.

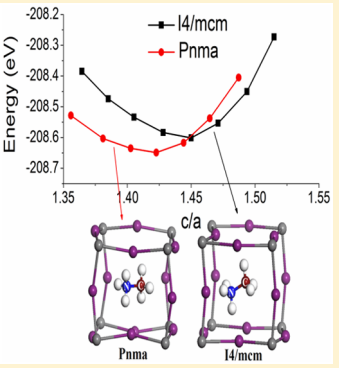

The organometal lead halide hybrid perovskite has recently been identified as a suitable candidate for use as active material in solar cells. Solar cell performance using this material has seen tremendous progress, from power conversion efficiency (PCE) of 3.8%[1] to above 16%[2] in a relatively short span of five years of dedicated photovoltaic research. Just recently, Zhou et al.[2] produced the highest performing solar cell to date with 19% PCE. Some properties are identified in these hybrid perovskites that could contribute to the efficacy of its use as active layer in solar cells, such as long carrier diffusion lengths,[3,4] large absorption coefficient,[5] low exciton binding energies,[6,7] and ferroelectricity.[8] Other interesting properties like thermoelectricity and [9] carrier screening effects[10] are under study. The suitability for solar cells to be fabricated economically using spin coating at low temperatures also makes these organometal lead halide perovskite solar cells commercially viable.

Perovskite is a structural class of materials having chemical structure ABX_3. In the case of organometal lead halide, perovskite A is the methylammonium cation $CH_3NH_3^+$ (denoted MA), B the Pb^{2+} ion and X is a halide ion studied. In the case of $MAPbI_3$, it exists as a 3-dimensional network of corner sharing PbI_6 octahedral with the MA cation occupying the spacing formed in the network. $MAPbI_3$ also exhibits structural phase transitions with decreasing temperature. Previously reported[11,12] $MAPbI_3$ takes on the cubic $Pm\bar{3}m$ structure above 327.4 K, then tetragonal *I4/mcm* at temperatures between 327.4 and 162.2 K, and below 162.2 K the orthorhombic *Pnma* phase. The orthorhombic phase of $MAPbI_3$ was originally assigned the polar space group $Pna2_1$ by Poglitsch and Weber,[13] but due to the absence of ferroelectric properties in this phase, the space group was hypothesized to be reassigned as *Pnma*.[14] This was subsequently confirmed by Baikie et al.[11] through single crystal X-ray diffraction of $MAPbI_3$ crystals at 100 K.

Computational studies[15−17] on $MAPbI_3$ structure elucidated the tetragonal structures proposed by Stoumpos et al. Notably, in the theoretical calculations by Mosconi et al.[15] using Perdew−Burke−Ernzerhof (PBE) exchange correlation functional, the tetragonal phase of the $MAPbI_3$ perovskite was computed in two different configurations, where both differs by the octahedra tilting and the relative cation orientation in the crystal. Filippetti et al.[18] computed the optical properties of $MAPbI_3$ and $MAPbI_2Cl$, but using different exchange correlation functional, the local density approximation (LDA). Geng et al.[19] have studied the tetragonal and orthorhombic phases of $MAPbI_3$ by using the PBE plus the nonlocal density functional vdW-DF based on experimental data and van Der Waals correction. Despite extensive computation on the various properties of perovskite, no systematic study has been done on the structural phase

Received: December 30, 2014
Accepted: February 3, 2015

DOI: 10.1021/jz502740d
J. Phys. Chem. Lett. 2015, 6, 681−685

transition between these two phases and the mechanism to change from one to another.

Strain engineering of materials through epitaxial growth has been a particularly effective approach for realizing new structures and properties of materials.[20−27] In this work, strain engineering has been applied in studying structural phase transitions between tetragonal *I*4/*mcm* and orthorhombic *Pnma* of $MAPbI_3$ perovskite structure under epitaxial strain by using ab initio calculations within different approximations. This study demonstrates the existence of critical ratio between out of plane and in-plane lattice parameter, *c*/*a*, which distinguishes the existence of the respective phases. The influence of strain on the rotation of MA cations is reported. Origin of the rotation is examined and identified, which is related to the tilt of PbI_6 octahedral and I−H bond.

The experiments report the *I*4/*mcm* tetragonal $MAPbI_3$ with lattice constants $a = b = 8.8$ Å and $c = 12.68$ Å[12,28] or $a = b = 8.85$ Å and $c = 12.44$ Å,[11] whereas for the *Pnma* orthorhombic $a = 8.84$ Å, $b = 8.56$ Å, and $c = 12.58$ Å.[11] Within our simulation to simplify the examination of the influence of biaxial epitaxial strain on the *Pnma* phase, we make an approximation with $a = b$ for the in-plane lattice constants. The lattice constants are shown in Table 1; here, the most stable structures are reported

Table 1. Lattice Constants of *I*4/*mcm* and *Pnma* $MAPbI_3$ within PBE and PBEsol Approximation

	a (Å)	*b* (Å)	*c* (Å)	*V* (Å^3)
*I*4/*mcm*				
PBE	8.94	8.94	12.82	1024.77
PBEsol	8.67	8.67	12.58	946.26
Exp	8.8	8.8	12.68	981.94[12,33]
	8.85	8.85	12.44	974.33[11]
Pnma				
PBE	8.94	8.94	12.59	1006.23
PBEsol	8.67	8.67	12.34	928.47
Exp	8.84	8.56	12.58	951.01[11]

in comparison to experiments. The results for *I*4/*mcm* and *Pnma* phase show that PBEsol gives a better agreement with experiments in comparison with PBE.

The effect of biaxial epitaxial strain on the $MAPbI_3$ within different approximations, PBE and PBEsol is shown in Figure 1a and b, respectively. The results show that the *Pnma* phase is the most stable phase which is in agreement with experimental reports. However, the phase transition between *Pnma* and *I*4/*mcm* in $MAPbI_3$ has not been found under compressive and tensile in-plane strain. In order to find the existence of the tetragonal *I*4/*mcm* structure, we notice that with the increase of the temperature the volume of crystal will increase and crystal may transform to other symmetries. Therefore, in order to understand the origin of the existence of tetragonal *I*4/*mcm* phase, we examine the influence of changing volume to the phase transition. In the PBE calculations in Figure 2a, a change in volume does not result in any phase transition between *I*4/*mcm* and *Pnma* phase but such phase transition is observed when the PBEsol approximation is applied, which supports the existence of *I*4/*mcm* phase under specific strain condition as shown in Figure 2b.

The PBEsol results in Figures 1b and 2b reflecting the change of the in-plane lattice constant a_{IP} or *a* and the volume suggest that the phase transition may due to the change in the out-of-plane lattice constant *c* rather than the in-plane lattice

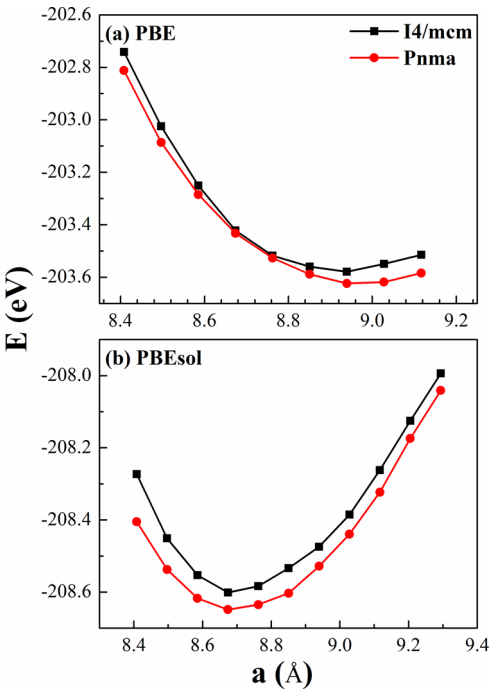

Figure 1. Influence of biaxial epitaxial strain on the change of in-plane lattice constant on the phase transition between *Pnma* and *I*4/*mcm* phase of $MAPbI_3$ within different approximation (a) PBE and (b) PBEsol.

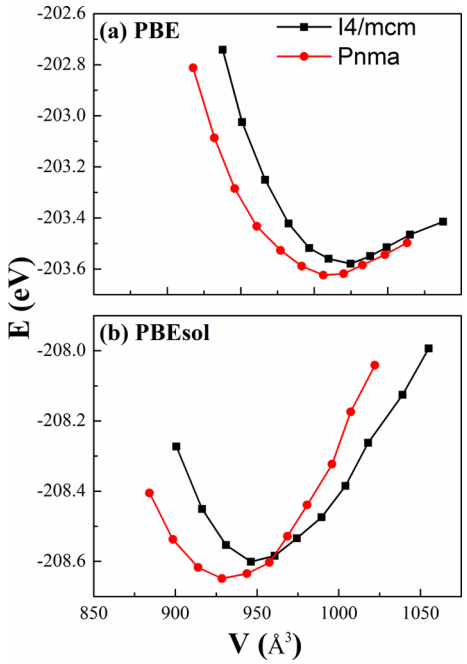

Figure 2. Influence of volume change to the phase transition of $MAPbI_3$ within different approximations, (a) PBE and (b) PBEsol.

constant *a*. To confirm this, we further examine the influence of this change to the phase transitions of $MAPbI_3$. The results are shown in Figure 3 (n.b. the lattice constant *a* is fully relaxed at each *c*). It is interesting to see that a change of lattice parameter *c* results in phase transition from orthorhombic *Pnma* to tetragonal *I*4/*mcm* phase at $c = 12.7$ and 12.44 Å corresponding to the PBE and PBEsol in Figure 3a and b, respectively. For perovskites, the ratio of out-of-plane to in-plane lattice

DOI: 10.1021/jz502740d
J. Phys. Chem. Lett. 2015, 6, 681−685

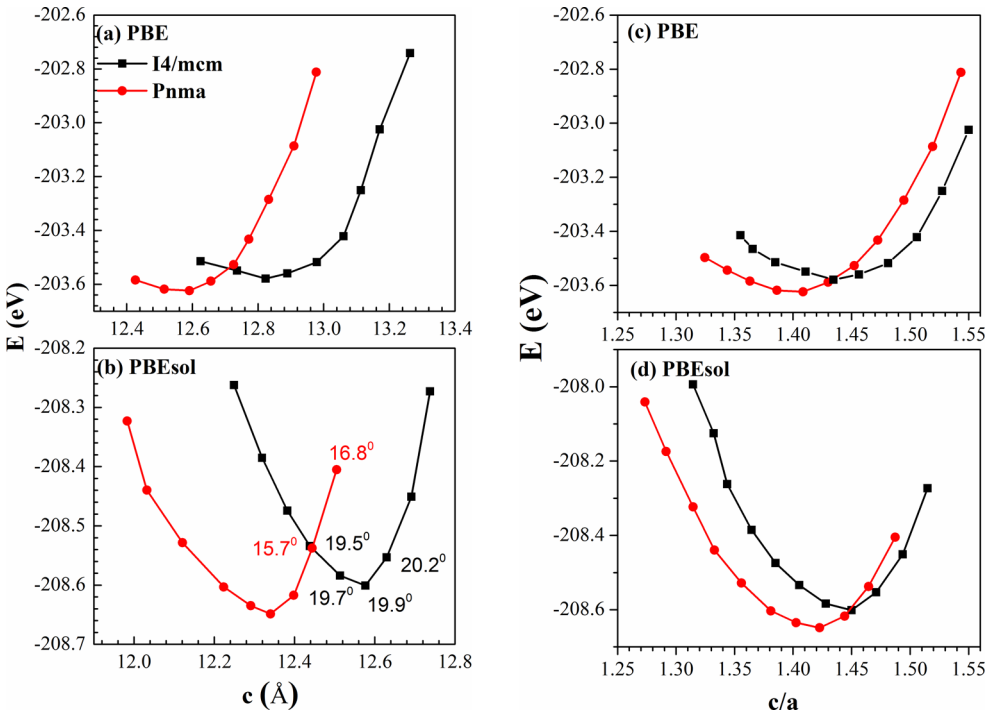

Figure 3. Influence of the change of, (a, b) out of plane lattice constant *c*, and (c, d) ratio *c*/*a* on the phase transition between orthorhombic *Pnma* and tetragonal *I*4/*mcm* in $MAPbI_3$ within different approximations PBE and PBEsol. The numbers in degree format of panel (b) represent the angle α, see text for detail.

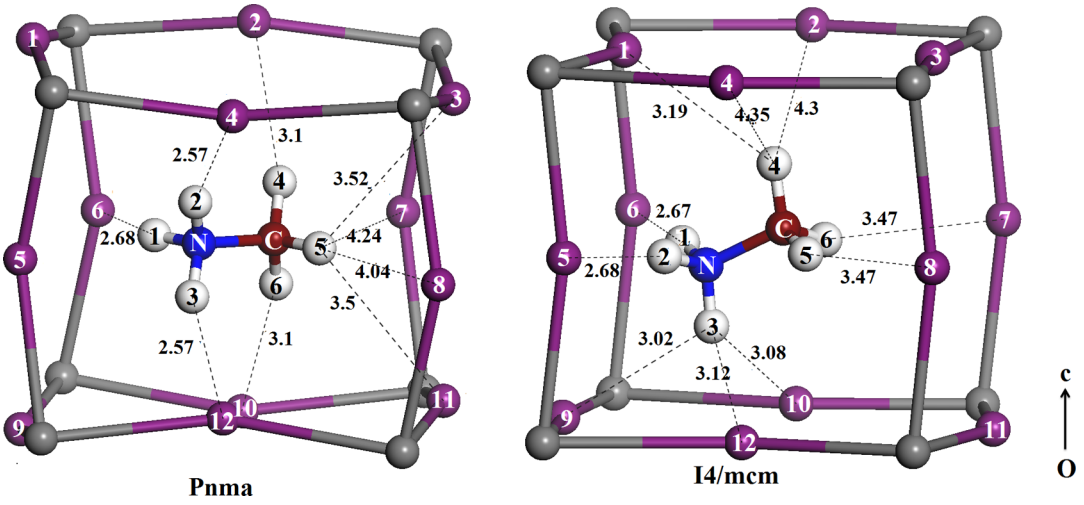

Figure 4. Analysis of the chemical bonds between I atoms and H atoms within different structure *Pnma* and *I*4/*mcm* at a = 8.98 Å and c = 12.57 Å (*I*4/*mcm*) and c = 12.30 Å (*Pnma*).

constants, *c*/*a*, is of particular interest for recognizing giant electronic polarization in perovskite oxides. Such dependence is now examined for $MAPbI_3$. Results are shown in Figure 3c and d within PBE and PBEsol approximations, respectively. Remarkably both PBE and PBEsol give almost the same critical *c*/*a* ratio 1.44 and 1.45, respectively. We notice here that within both PBE and PBEsol approximations the phase transition takes place at the critical *c*/*a* ratio beyond which the *I*4/*mcm* phase is the more stable structure shown in Figure 3c and d. The $MAPbI_3$ is stabilized with orthorhombic *Pnma* phase and tetragonal *I*4/*mcm* phase at low and high *c*/*a* ratio (*c*/*a* ∼ 1.45) respectively. This remarkable result indicates that $MAPbI_3$ could be a ferroelectric material with a giant polarization in the tetragonal phase.

The tetragonal *I*4/*mcm* of $MAPbI_3$ has an antiphase tilt (Glazer's notation: $a^0a^0c^-$) along the *c* direction, whereas the orthorhombic *Pnma* phase has an in-phase tilt along the *c* axis but antiphase tilt in other directions, (Glazer's notation: $a^-b^-c^+$). Our study shows that in the tetragonal *I*4/*mcm* phase, the MA cations orient mainly in the (111) direction but in the orthorhombic phase they mainly lie in the Oxy plane. Within the PBEsol approximation, going from tetragonal to orthorhombic phase the angle α, defined as the angle between the Oxy plane and MA cation, is slowly reduced from 20.2° at c = 12.64 Å to 19.5° at intersection point c_{int} =12.44 Å, as shown in Figure 3b. At c_{int}, changing from tetragonal phase to orthorhombic phase results in the decrease of α from 19.5° (*I*4/*mcm*) to 15.7° (*Pnma*). In the orthorhombic *Pnma* phase,

DOI: 10.1021/jz502740d
J. Phys. Chem. Lett. 2015, 6, 681−685

the angle α increases when $c > c_{int}$ implying that the *Pnma* phase is not stable when $c/a > 1.45$. When $c < 12.34$ Å, the MA cations mainly lie in the Oxy plane, that is $\alpha \sim 0°$ shown in Figure 3. These results emphasize that the *Pnma* phase is stable with MA cations lying in the Oxy plane. Therefore, this observation tells us that a change in c/a ratio results in the rotation of MA cations from in-plane at low c/a to out-of-plane when $c > 12.34$ Å.

To understand the origin of rotations in MA cations within orthorhombic *Pnma* and tetragonal *I4/mcm* phases we analyze the chemical bonds in $MAPbI_3$. Our examination shows that the I−H bonds play an important role on the rotation as shown in Figure 4. In the *Pnma* phase the atom H1 in the NH_3 component of the MA cation bonds to atom I6, whereas the other two H atoms, H2 and H3, bond to I4 and I12, respectively. In the CH_3 component of the MA cation, atom H6 bonds to atom I10, atom H4 to atom I2, and atom H5 to two I atoms, I3 and I11. Hydrogen atoms in CH_3 component have much weaker bonds to the I atoms in comparison to those in the NH_3 component. These I−H bonds force the MA cations to lie in the Oxy plane within the *Pnma* structure. However, varying the phase from *Pnma* to *I4/mcm* changes the octahedral tilting of PbI_6 along the Oz from in-phase tilt to antiphase tilt. Such change in tilting brings some I1, I5 atoms nearer to the MA cations resulting in a rotation of MA cations about the N atoms. More specifically, atom H2 bonds to atom I5 instead of atom I4 and atom H3 now has much weaker bond to the I atoms, bonding to three I atoms, I9, I10, and I12. Such rotation shifts the CH_3 component and brings atom H4 near to atom I1, changing the I2−H4 bond in *Pnma* structure to I1−H4 bond in the *I4/mcm* structure. Such rotation makes atom H6 bonds to atom I7 and atom H5 bonds to atom I8 instead of atoms I10 and I3, and atom I11 in *Pnma* phase, respectively. *The I1−H4 bond makes the MA cations rotate out of plane to lie along the [111] direction*. We notice here that in both *I4/mcm* and *Pnma* structures, the NH_3 component bonds strongly to I atoms with I−H bond lengths are about ∼2.6−2.7 Å. *A change of lattice constants will not result in a significant change in this I−H bond length*. In contrast, the CH_3 components have much weaker bonding to I atoms. Varying the lattice constants changes the I−H bond lengths with H atoms from the CH_3 components. *Therefore, an increase of lattice parameter c rotates the MA cations in and out of Oxy plane about the NH_3 component. Because of this, the MA cation does not freely rotate within the cuboctahedral cavity formed by the inorganic cage; instead, it precesses about the NH_3 component.*

In conclusion, we have examined the influence of epitaxial strain on the phase transition of $MAPbI_3$. What we have observed is that a change of the in-plane lattice constants does not result in any phase transition from orthorhombic *Pnma* to tetragonal *I4/mcm* phase while varying the lattice constant c results in the phase transition between these two phases. Closer examination shows that the ratio c/a plays a key role in this phase transition. A change in c/a ratio results in the rotation of MA cations about NH_3 component in and out of Oxy plane leading to the phase transition. The orthorhombic *Pnma* phase is stable at $c/a < 1.45$, whereas the tetragonal *I4/mcm* phase is stabilized at high c/a ratio, $c/a > 1.45$ implying that tetragonal $MAPbI_3$ could be a ferroelectric with a giant electronic polarization. The study of H−I bond lengths also shows that the MA cation precesses about the NH_3 component, instead of freely rotating within the cuboctahedral cavity formed by the inorganic cage. Our study guides the solar cell community to explore possible conditions for the existence of orthorhombic *Pnma* phase or tetragonal *I4/mcm* phase in $MAPbI_3$ to utilize beneficial properties in these different structural phases.

For the electronic structures of $MAPbI_3$ calculations, we use an all-electron-like projector augmented wave (PAW) method[29] with the Perdew−Burke−Ernzerhof (PBE)[30] and PBE revised for solids (PBEsol)[31] exchange correlation potential as implemented in the VASP code.[32] The cutoff energy for the plane wave expansion of the wave functions is 500 eV, and all atoms in the unit cell are fully relaxed until the Hellman-Feynman forces are less than 0.01 eV/Å. The 3 × 2 × 3 Monkhorst−Pack grid of k-points[33] for Brillouin zone integration was used in calculations. The semicores of Pb atoms are treated as valence electrons; that is, 14 valence electrons for Pb ($5d^{10}$ $6s^2$ $6p^2$). The I-$5s^2 5p^5$, C-$2s^2 2p^2$, N-$2s^2 2p^3$, and H-1s were considered as valence electrons.

To study the effect of epitaxial strain on $MAPbI_3$, we employ a 48-atom unit cell with lattice vectors $\mathbf{a_1} = a_{IP}\mathbf{x}$, $\mathbf{a_2} = a_{IP}\mathbf{y}$ and $\mathbf{a_3} = c\mathbf{z}$; here, a_{IP} is the in-plane lattice constant and c is fully optimized.

AUTHOR INFORMATION

Corresponding Author

*E-mail: ongpk@ihpc.a-star.edu.sg.

Notes

The authors declare no competing financial interest.

ACKNOWLEDGMENTS

This work was supported by Institute of High Performance Computing, Agency of Science, Technology, And Research (A*STAR). K.P.O. would like to thank Prof. Subodh Mhaisalkar, Prof. Nripan Mathews, and Prof. Sum Tze Chien for information and fruitful discussions on hybrid perovskites. Work at Nanyang Technological University (NTU) was supported by NTU Research Student Scholarship (NTU-RSS).

REFERENCES

(1) Kojima, A.; Teshima, K.; Shirai, Y.; Miyasaka, T. Organometal Halide Perovskites as Visible-Light Sensitizers for Photovoltaic Cells. *J. Am. Chem. Soc.* **2009**, *131*, 6050−6051.

(2) Zhou, H.; Chen, Q.; Li, G.; Luo, S.; Song, T.-b.; Duan, H.-S.; Hong, Z.; You, J.; Liu, Y.; Yang, Y. Interface Engineering of Highly Efficient Perovskite Solar Cells. *Science* **2014**, *345*, 542−546.

(3) Xing, G.; Mathews, N.; Sun, S.; Lim, S. S.; Lam, Y. M.; Gratzel, M.; Mhaisalkar, S.; Sum, T. C. Long-Range Balanced Electron- and Hole-Transport Lengths in Organic-Inorganic $CH_3NH_3PbI_3$. *Science* **2013**, *342*, 344−347.

(4) Stranks, S. D.; Eperon, G. E.; Grancini, G.; Menelaou, C.; Alcocer, M. J. P.; Leijtens, T.; Herz, L. M.; Petrozza, A.; Snaith, H. J. Electron-Hole Diffusion Lengths Exceeding 1 Micrometer in an Organometal Trihalide Perovskite Absorber. *Science* **2013**, *342*, 341−344.

(5) Singh, S. P.; Nagarjuna, P. Organometal Halide Perovskites As Useful Materials In Sensitized Solar Cells. *Dalton Trans.* **2014**, *43*, 5247.

(6) Sun, S.; Salim, T.; Mathews, N.; Duchamp, M.; Boothroyd, C.; Xing, G.; Sum, T. C.; Lam, Y. M. The Origin of High Efficiency on Low-Temperature Solution-Processable Bilayer Organometal Halide Hybrid Solar Cells. *Energy Environ. Sci.* **2014**, *7*, 399.

(7) D'Innocenzo, V.; Grancini, G.; Alcocer, M. J. P.; Kandada, A. R. S.; Stranks, S. D.; Lee, M. M.; Lanzani, G.; Snaith, H. J.; Petrozza, A. Excitons Versus Free Charges in Organo-Lead Tri-Halide Perovskites. *Nat. Commun.* **2014**, *5*, 3586.

(8) Frost, J. M.; Butler, K. T.; Brivio, F.; Hendon, C. H.; van Schilfgaarde, M.; Walsh, A. Atomistic Origins of High-Performance in

DOI: 10.1021/jz502740d
J. Phys. Chem. Lett. 2015, 6, 681−685

Hybrid Halide Perovskite Solar Cells. *Nano Lett.* **2014**, *14*, 2584−2590.
(9) He, Y.; Galli, G. Perovskites for Solar Thermoelectric Applications: a First Principle Study of $CH_3NH_3AI_3$ (*a* = Pb and Sn). *Chem. Mater.* **2014**, *26*, 5394−5400.
(10) Even, J.; Pedesseau, L.; Katan, C. Analysis of Multi-Valley and Multi-Bandgap Absorption and Enhancement of Free Carriers Related to Exciton Screening in Hybrid Perovskites. *J. Phys. Chem. C* **2014**, *118*, 11566−11572.
(11) Baikie, T.; Fang, Y.; Kadro, J. M.; Schreyer, M.; Wei, F.; Mhaisalkar, S. G.; Graetzel, M.; White, T. J. Synthesis and Crystal Chemistry of the Hybrid Perovskite $(CH_3NH_3)PbI_3$ for Solid-State Sensitised Solar Cell Applications. *J. Mater. Chem. A* **2013**, *1*, 5628−5641.
(12) Kawamura, Y.; Mashiyama, H.; Hasebe, K. Structural Study on Cubic-Tetragonal Transition of $CH_3NH_3PbI_3$. *J. Phys. Soc. Jpn.* **2002**, *71*, 1694−1697.
(13) Poglitsch, A.; Weber, D. Dynamic Disorder in Methylammoniumtrihalogenoplumbates (II) Observed by Millimeter-Wave Spectroscopy. *J. Chem. Phys.* **1987**, *87*, 6373−6378.
(14) Swainson, I.; Hammond, R.; Soulliere, C.; Knop, O.; Massa, W. Phase Transitions in the Perovskite Methylammonium Lead Bromide, $CH_3ND_3PbBr_3$. *J. Solid State Chem.* **2003**, *176*, 97−104.
(15) Mosconi, E.; Amat, A.; Nazeeruddin, M. K.; Gratzel, M.; De Angelis, F. First-Principles Modeling of Mixed Halide Organometal Perovskites for Photovoltaic Applications. *J. Phys. Chem. C* **2013**, *117*, 13902−13913.
(16) Colella, S.; Mosconi, E.; Fedeli, P.; Listorti, A.; Gazza, F.; Orlandi, F.; Ferro, P.; Besagni, T.; Rizzo, A.; Calestani, G.; et al. $MAPbI_{3-x}Cl_x$ Mixed Halide Perovskite for Hybrid Solar Cells: The Role of Chloride as Dopant on the Transport and Structural Properties. *Chem. Mater.* **2013**, *25*, 4613−4618.
(17) Quarti, C.; Grancini, G.; Mosconi, E.; Bruno, P.; Ball, J. M.; Lee, M. M.; Snaith, H. J.; Petrozza, A.; Angelis, F. D. The Raman Spectrum of the $CH_3NH_3PbI_3$ Hybrid Perovskite: Interplay of Theory and Experiment. *J. Phys. Chem. Lett.* **2014**, *5*, 279−284.
(18) Filippetti, A.; Mattoni, A. Hybrid Perovskites For Photovoltaics: Insights From First Principles. *Phys. Rev. B* **2014**, *89*, 125203.
(19) Geng, W.; Zhang, L.; Zhang, Y.-N.; Lau, W.-M.; Liu, L.-M. First-principle Study of Lead Iodide Perovskite Tetragonal and Orthorhombic Phases for Photovoltaics. *J. Phys. Chem. C* **2014**, *118*, 19565−19571.
(20) Locquet, J.-P.; Perret, J.; Fompeyrine, J.; Machler, E.; Seo, J. W.; Van Tendeloo, G. Doubling the Critical Temperature of $La_{1.9}Sr_{0.1}CuO_4$ Using Epitaxial Strain. *Nature* **1998**, *394*, 453−456.
(21) Choi, K. J.; Biegalski, M.; Li, Y.; Sharan, A.; Schubert, J.; Uecker, R.; Reiche, P.; Chen, Y.; Pan, X.; Gopalan, V.; et al. Enhancement of Ferroelectricity in Strained $BaTiO_3$ Thin Films. *Science* **2004**, *306*, 1005−1009.
(22) Lee, J. H.; Fang, L.; Vlahos, E.; Ke, X.; Jung, Y. W.; Kourkoutis, L. F.; Kim, J.-W.; Ryan, P. J.; Heeg, T.; Roeckerath, M.; et al. A Strong Ferroelectric Ferromagnet Created by Means of Spin-Lattice Coupling. *Nature* **2010**, *466*, 954−958.
(23) Smith, A. M.; Mohs, A. M.; Nie, S. Tuning the Optical and Electronic Properties of Colloidal Nanocrystals by Lattice Strain. *Nat. Nanotechnol.* **2008**, *4*, 56−63.
(24) Dupe, B.; Prosandeev, S.; Geneste, G.; Dkhil, B.; Bellaiche, L. $BiFeO_3$ Films Under Tensile Epitaxial Strain from First Principles. *Phys. Rev. Lett.* **2011**, *106*, 237601.
(25) Schlom, D. G.; Chen, L.-Q.; Eom, C.-B.; Rabe, K. M.; Streiffer, S. K.; Triscone, J.-M. Strain Tuning of Ferroelectric Thin Films. *Annu. Rev. Mater. Res.* **2007**, *37*, 589−626.
(26) Fan, Z.; Wang, J.; Sullivan, M. B.; Huan, A.; Singh, D. J.; Ong, K. P. Structural Instability of Epitaxial (001) $BiFeO_3$ Thin Films under Tensile Strain. *Sci. Rep.* **2014**, *4*, 4631.
(27) Wang, J.; Neaton, J.; Zheng, H.; Nagarajan, V.; Ogale, S.; Liu, B.; Viehland, D.; Vaithyanathan, V.; Schlom, D.; Waghmare, U.; et al. Epitaxial $BiFeO_3$ Multiferroic Thin Film Heterostructures. *Science* **2003**, *299*, 1719−1722.
(28) Lee, M. M.; Teuscher, J.; Miyasaka, T.; Murakami, T. N.; Snaith, H. J. Efficient Hybrid Solar Cells Based on Meso-Superstructured Organometal Halide Perovskites. *Science* **2012**, *338*, 643−647.
(29) Blochl, P. E. Projector Augmented-Wave Method. *Phys. Rev. B* **1994**, *50*, 17953.
(30) Perdew, J. P.; Burke, K.; Ernzerhof, M. Generalized Gradient Approximation Made Simple. *Phys. Rev. Lett.* **1996**, *77*, 3865.
(31) Perdew, J. P.; Ruzsinszky, A.; Csonka, G. I.; Vydrov, O. A.; Scuseria, G. E.; Constantin, L. A.; Zhou, X.; Burke, K. Restoring the Density-Gradient Expansion for Exchange in Solids and Surfaces. *Phys. Rev. Lett.* **2008**, *100*, 136406.
(32) Kresse, G.; Furthmuller, J. Efficient Iterative Schemes for Ab Initio Total-Energy Calculations Using a Plane-Wave Basis Set. *Phys. Rev. B* **1996**, *54*, 11169.
(33) Monkhorst, H. J.; Pack, J. D. Special Points for Brillouin-Zone Integrations. *Phys. Rev. B* **1976**, *13*, 5188.

DOI: 10.1021/jz502740d
J. Phys. Chem. Lett. 2015, 6, 681−685